Chemical Engineering Journal 159 (2010) 242–246

Contents lists available at ScienceDirect

Chemical Engineering Journal

journal homepage: www.elsevier.com/locate/cej

Correlations of WO_3 species and structure with the catalytic performance of the selective oxidation of cyclopentene to glutaraldehyde on WO_3/TiO_2 catalysts

Guang Lu [a], Xinyong Li [a,b,*], Zhenping Qu [a], Qidong Zhao [a], Hong Li [a], Yu Shen [a], Guohua Chen [b]

[a] Key Laboratory of Industrial Ecology and Environmental Engineering, State Key Laboratory of Fine Chemicals, School of Environmental Science & Technology, Dalian University of Technology, Dalian 116024, China
[b] Department of Chemical Engineering, The Hong Kong University of Science & Technology, Clear Water Bay, Kowloon, Hong Kong, China

ARTICLE INFO

Article history:
Received 26 August 2009
Received in revised form 9 February 2010
Accepted 15 February 2010

Keywords:
WO_3/TiO_2
TiO_2 microsphere
Cyclopentene
Selective oxidation
H_2O_2

ABSTRACT

A series of WO_3/TiO_2 catalysts were synthesized by ultrasonic impregnation method using as-prepared TiO_2 microspheres as support as a function of tungsten oxide species loading. The crystalline structure, molecular structure and the interaction with the support of the supported tungsten oxide phase were characterized by various techniques (scanning electron microscope (SEM), transmission electron microscope (TEM), X-ray diffraction (XRD), Raman, X-ray photoelectron spectroscopy (XPS) and specific surface areas (BET)), and their effects on the catalytic performance in selective oxidation of cyclopentene to glutaraldehyde were investigated. It was found that highly dispersed WO_3 species were obtained on the surface of TiO_2, and only W(VI) oxidation state was present on the support. The WO_3/TiO_2 catalysts showed high catalytic activity for selective oxidation of cyclopentene to glutaraldehyde. The catalytic activity increased with the WO_3 loading, and reached maximum on the catalysts with the WO_3 loading of 15–20 wt%. The molecular structures of calcinated tungsten oxide phase were determined to be tetrahedral surface tungsten oxide species with the WO_3 loading below 20 wt%, and both Brönsted acid sites and Lewis acid sites were present on the surface of the catalysts. The strong support effect on the dispersion and molecular structure of WO_3 as well as the Brönsted acid observed in the present work may have important catalytic implication. Further increasing the WO_3 loading resulted in the decrease of catalytic performance of the catalyst, meanwhile the crystalline WO_3 nanoparticles were present on the surface of the support. These reactivity trends showed the influence of molecular structure of WO_3 on the surface of TiO_2 support on the selective oxidation activity of cyclopentene to glutaraldehyde.

1. Introduction

Glutaraldehyde (GA) is widely used as a disinfectant bactericide in many fields such as the tanning process of leather, environmental protection, water treatment, etc. [1,2]. However, the commercial syntheses of GA is mainly based on a multi-step process using expensive propenal and vinyl ethyl ether as starting materials, which results in the high cost of GA and constrains the potential application of GA [3,4]. Therefore, it has been necessary to develop more effective process for the synthesis of GA. An alternative way to produce GA is the selective oxidation of cyclopentene (CPE) using environmentally friendly aqueous H_2O_2 as the oxidant [5], since a great quantity of CPE could be easily obtained by the selective hydrogenation of cyclopentadiene. In this reaction system, a large number of W-containing homogeneous catalysts (WO_3/SiO_2, WO_3/TiO_2-SiO_2, W-MCM-41, W-MCM-48 WO_3/TiO_2 and W-SBA-15) have been investigated [6–11]. Higher selectivity of GA could be obtained for the samples with significant surface acidic sites (Brönsted acid sites and Lewis acid sites) [12]. And high dispersion of tungsten species on the surface of support was proposed to be helpful to the catalytic performance of GA [13–15].

The states of tungsten oxide species formed on the catalyst, depending on the loading amount of tungsten oxide, play a crucial role in their overall catalytic performance. The tungsten oxide species were mainly in the tetrahedrally coordinated states at low WO_3 loadings and higher loading of WO_3 leaded to the formation of the distorted octahedrally coordinated species of tungsten oxide on the surface of catalyst [16]. It has been reported that the tetrahedrally coordinated tungsten oxide species were the active centers in the butane-1 metathesis application [17]. However, the relationship of these different tungsten oxide states with their catalytic active is not fully expatiated for the oxidation of CPE to GA at present.

In this work, TiO_2 microspheres were fabricated by the hydrothermal precipitation procedure with $TiCl_4$ as the starting

* Corresponding author at: Key Laboratory of Industrial Ecology and Environmental Engineering, State Key Laboratory of Fine Chemicals, School of Environmental Science & Technology, Dalian University of Technology, Dalian 116024, China. Tel.: +86 411 8470 7733; fax: +86 411 8470 8084.
E-mail address: xyli@dlut.edu.cn (X. Li).

1385-8947/$ – see front matter © 2010 Elsevier B.V. All rights reserved.
doi:10.1016/j.cej.2010.02.024

material in the presence of H_2O and urea. And WO_3/TiO_2 catalysts were prepared using a novel ultrasonic impregnation method that could well predigest the preparation procedures and lower the preparation cost. The influence of tungsten oxide loadings on the catalytic activity of CPE selective oxidation to GA over WO_3/TiO_2 catalysts was investigated and the relationship of the different tungsten oxide states to their catalytic performance was initially correlated.

2. Experimental

2.1. Catalyst preparation

2.1.1. Preparation of the titania microspheres

TiO_2 microspheres were prepared by the hydrothermal precipitation procedure with $TiCl_4$ as the starting material. 2 ml $TiCl_4$ was added dropwise into a mixture consisting of 30 ml anhydrous ethanol and equal amounts of distilled water at room temperature under sonication conditions. Then 6 g urea and 2.2 g $(NH_4)_2SO_4$ were added in the above mixture. A transparent solution was obtained after sonication for 2–4 h, and then the mixture was transferred into a 100 ml autoclave, where it was heated and maintained at 383 K for 2 h. Then the autoclave was cooled to room temperature naturally. Subsequently, the resultant slurry was filtered, washed twice with distilled water and three times with absolute ethanol. Finally, the produced sample was vacuum-dried at 353 K for 12 h and calcined at 773 K for 3 h.

2.1.2. Preparation of the WO_3/TiO_2 catalyst

The WO_3/TiO_2 catalysts with different WO_3 loadings from 5 to 30 wt% were prepared by ultrasonic impregnation method. The required amount of ammonium tungstate was dispersed in distilled water. The as-synthesized titania microspheres were added into the sonication solution at 343 K under sonication powers of 480 W overnight, and the water was completely evaporated. The prepared catalyst was obtained after drying at 393 K for 12 h and calcination in a muffle oven at 773 K for 5 h.

2.2. Characterization

Specific surface areas (BET) and mean cylindrical pore diameters were determined by nitrogen physisorption at 77 K using a Micromeritics ASAP 2000 instrument.

Scanning electron microscopy (SEM) analysis was conducted with a JSM-6700 LV electron microscope operating at 5.0 kV. Transmission electron microscopy (TEM) image was performed by a Tecnai $G^2$20 transmission electron microscope at an accelerating voltage of 200 kV.

X-ray diffraction (XRD) patterns of WO_3/TiO_2 samples were obtained on a XRD-6000 diffractometer using Cu Kα as radiation (λ = 1.5406 nm) over the 2θ range of 20–80° at 2°/min, which was operated at 30 mA and 40 kV.

X-ray photoelectron spectroscopy (XPS) spectra of WO_3/TiO_2 samples were recorded on a Sigma Probe Instrument (Thermo VG, U.K.), in which standard monochromatic Al Kα excitation was 1486.6 eV. The base pressure of the test chamber was below 5×10^{-9} Torr at room temperature. Measurements were obtained at the pass energy of 93.90 eV. All binding energies were calibrated using contaminant carbon (C_{1s} = 284.6 eV) as a reference.

The Raman experiments were performed under ambient conditions on Jobin Yvon T-64000 taking holographic notch as filter, symphony liquid nitrogen cooled CCD as detector and air-cooled argon ion as laser. The excitation line of the Raman scattering was 532 nm and the laser power at the sample was about 4 mV. The scan time was 120 s.

Table 1
Textural property of the samples.

WO_3 loading (wt%)	BET ($m^2\ g^{-1}$)	Vp ($cm^3\ g^{-1}$)	dp (nm)
5 wt% WO_3/TiO_2	195	0.22	4.9
10 wt% WO_3/TiO_2	184	0.21	5.0
15 wt% WO_3/TiO_2	167	0.20	5.2
20 wt% WO_3/TiO_2	142	0.19	5.3
30 wt% WO_3/TiO_2	98	0.15	5.8

The FT-IR spectra of chemisorbed pyridine (Py-IR) were obtained on a Nicolet Model 205 spectrophotometer using thermo electrically cooled deuterated triglycene sulphate (DTGS) detector. For the infrared absorption spectra, the samples were pressed into pellets. Then the sample pellets were outgassed at 623 K for 1 h prior to pyridine adsorption. After the adsorption of pyridine at room temperature, the catalysts were outgassed at 473 K and their spectra were recorded in the wave-number region of 1400–1700 cm^{-1}.

2.3. Activity test

The oxidation of CPE was performed at 308 K for 24 h with vigorous stirring in a regular glass using tert-butanol (*t*-BuOH) as the solvent and 50 wt% aqueous H_2O_2 as the oxidant, as reported in Ref. [18]. WO_3/TiO_2 of 1 g, *t*-BuOH of 20 ml, CPE of 2 ml and 50 wt% aqueous H_2O_2 of 3 ml were required in the activity test. The conversion of CPE and the yield of GA were determined by gas chromatograph with FID detector using toluene as an internal standard. And the remaining amount of hydrogen peroxide was determined by the iodometric titration.

3. Results and discussion

3.1. Characterizations of the titania microsphere and WO_3/TiO_2 catalyst

The surface area, porosity and pore diameter of the WO_3/TiO_2 catalysts with different WO_3 loadings are summarized in Table 1. It is shown that the surface area and porosity (Vp) of WO_3/TiO_2 catalysts with WO_3 loading <20 wt% decrease slightly, indicating that WO_3 would be dispersed well on the surface of titania microspheres. However, when WO_3 loading is higher than 20 wt%, the surface area of the sample is reduced greatly, and the excess content of tungsten species leads them to aggregation, which also brings the decrease of the porosity of catalyst.

The SEM images and EDS spectra of the titania support and the WO_3/TiO_2 (20 wt%) catalyst calcined at 773 K are shown in Fig. 1, and the spherical particles are obtained for the two samples. The SEM images indicate that the average sizes of the TiO_2 microsphere and WO_3/TiO_2 (20 wt%) sample are about 4.8 and 5.1 μm, respectively. The chemical composition determined by the EDS spectra shows that the titania particles are composed of Ti and O atoms, and the WO_3/TiO_2 catalyst is composed of Ti, W and O atoms. When tungsten oxides species are supported on the titania spheres, the characteristic structure of the microspheres is still maintained. Meanwhile, the sphere surface that is constituted of Ti, W and O atoms keeps relatively smooth, indicating WO_3 with 20 wt% loading are well dispersed on the surface of TiO_2 microsphere [19].

The XRD patterns of WO_3/TiO_2 catalysts with various WO_3 loadings are shown in Fig. 2. The diffraction patterns of anatase TiO_2 with five peaks at 2θ = 25.3°, 37.9°, 47.9°, 54.3° and 62.5° are found for all samples and no obvious change for their intensity is observed. These results reveal that the anatase phase of the titania microsphere can not be changed after the impregnation of tungsten oxide, regardless of the WO_3 loadings [10,20]. When the WO_3 load-

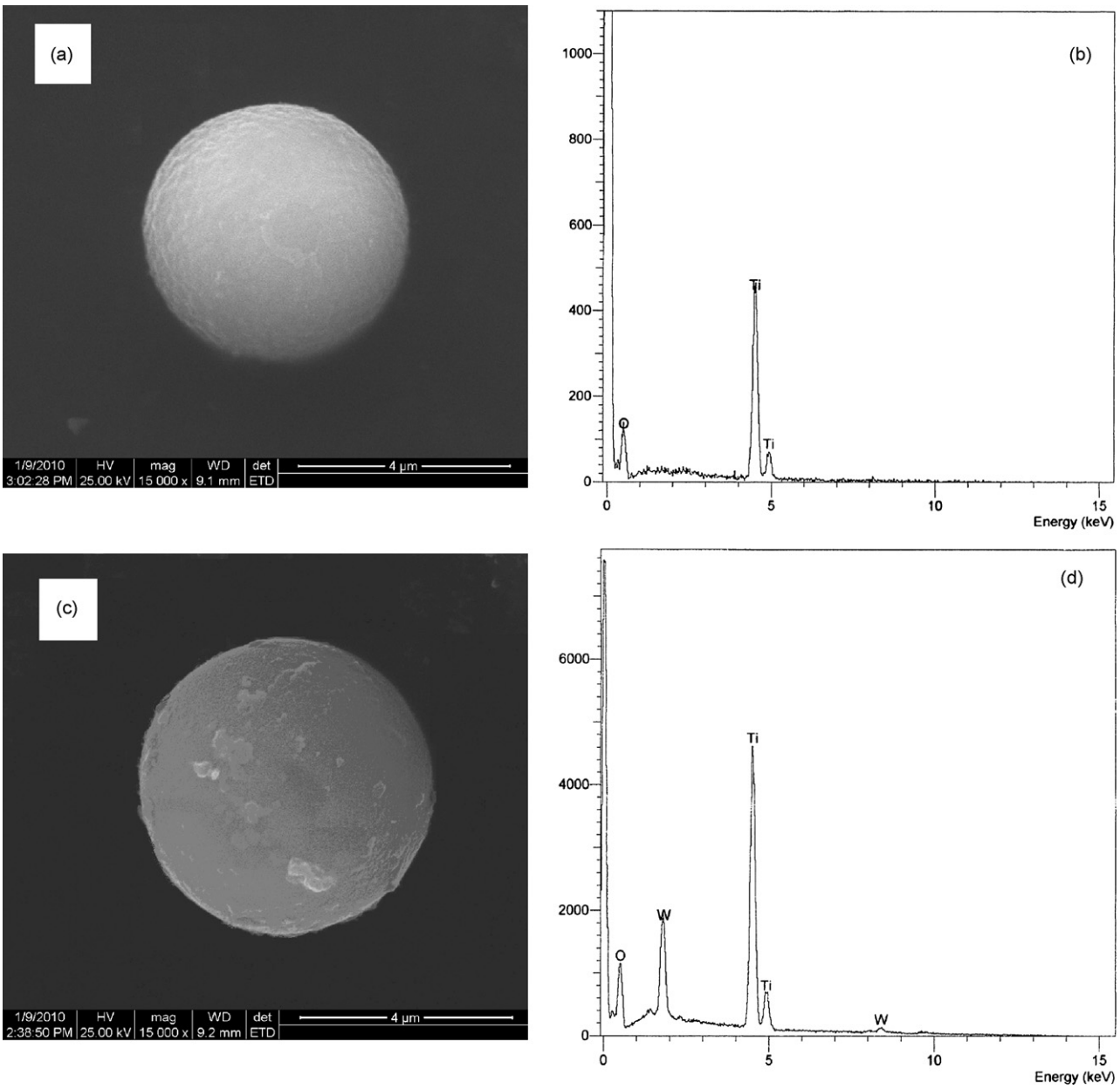

Fig. 1. SEM images of one of the TiO_2 microspheres (a) and the 20 wt% WO_3/TiO_2 catalyst (c), and EDS image of the TiO_2 (b) 20 wt% WO_3/TiO_2 sample (d).

ing is less than 20 wt%, no peaks corresponding to the crystalline phase of WO_3 is observed for WO_3/TiO_2 samples, indicating WO_3 is highly dispersed on the surface of the catalyst. Whereas, when the WO_3 loading exceeds 20 wt%, the characteristic peaks of crystalline WO_3 appear and their intensities increase with the increasing of the tungsten oxide contents.

XPS spectra of the WO_3/TiO_2 samples with different WO_3 loadings provide the information on the chemical states and relative quantities of outermost surface compounds. The XPS spectra taken in the Ti 2p region (not shown here) of the WO_3/TiO_2 samples show two peaks with binding energies centered at about 465 eV ($2p_{1/2}$) and 459 eV ($2p_{3/2}$), respectively, corresponding to the Ti^{4+} oxidation state [21]. The XPS spectra recorded in the W 4f region (Fig. 3) show two peaks with binding energies centered at about 35.6 eV ($4f_{7/2}$) and 37.7 eV ($4f_{5/2}$), corresponding to tungsten in the W^{6+} oxidation state [22]. These peaks are asymmetric due to overlapping with the Ti 3p component [23]. With the increase of WO_3 loading, the intensities of W 4f peaks and the W^{6+} surface concentration increase. In addition, WO_x surface coverage linearly correlates to the WO_x surface density (W/(W + Ti)) for the catalysts with WO_3 loading $\leq$20 wt%, as showed in the inset of Fig. 3, which suggests that WO_x is well dispersed on the surface of TiO_2 microsphere and there exists a strong interaction between WO_3 and TiO_2 when the loading of WO_3 is lower than 20 wt% [23].

The Raman spectra of WO_3/TiO_2 samples with different WO_3 loadings are shown in Fig. 4. The bands at around 144, 199, 399, 510 and 643 cm^{-1} originate from the anatase phase of TiO_2 [8,24]. No obvious change for these bands after loading tungsten oxide on the support, which is in agreement with the results of XRD. For the WO_3/TiO_2 samples with WO_3 loading <15 wt%, no new Raman band appears except for those characteristic peaks of anatase, which is different from the previously reported literature [16,18]. The strong chemical interaction between the highly dispersed WO_x species and the TiO_2 oxide clusters may be the cause of no observation of surface WO_x band. When the WO_3 loading increases to 15 wt%, an additional band at about 965 cm^{-1} is found and its inten-

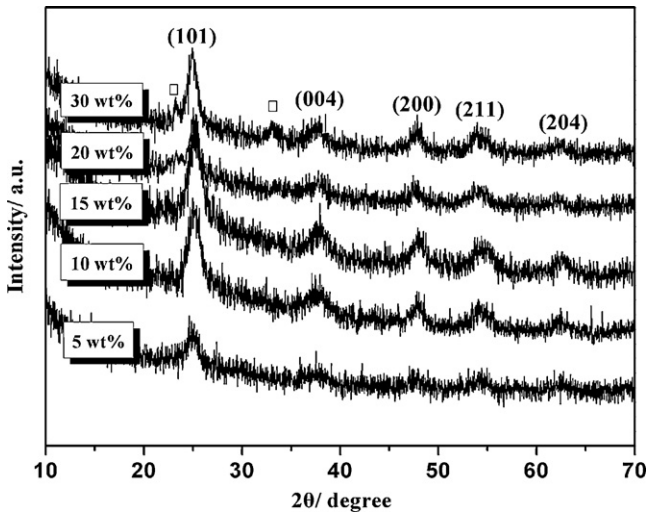

Fig. 2. XRD patterns of WO_3/TiO_2 catalysts with different WO_3 loadings (□, WO_3 crystal).

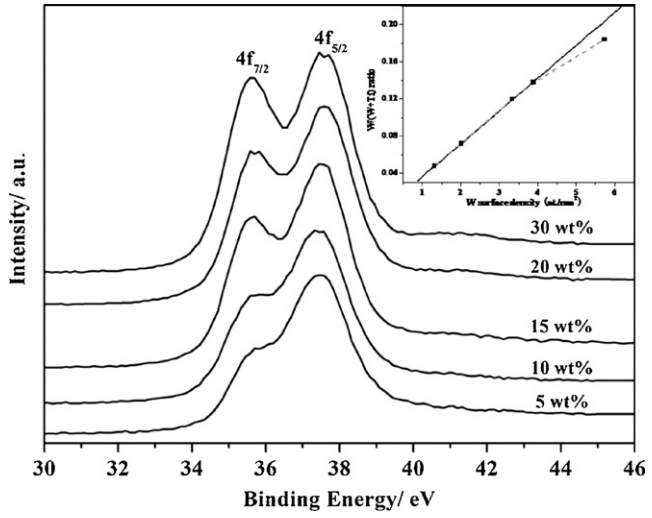

Fig. 3. XPS spectra of W 4f and W surface density versus W surface coverage (inset) of different WO_3/TiO_2 samples.

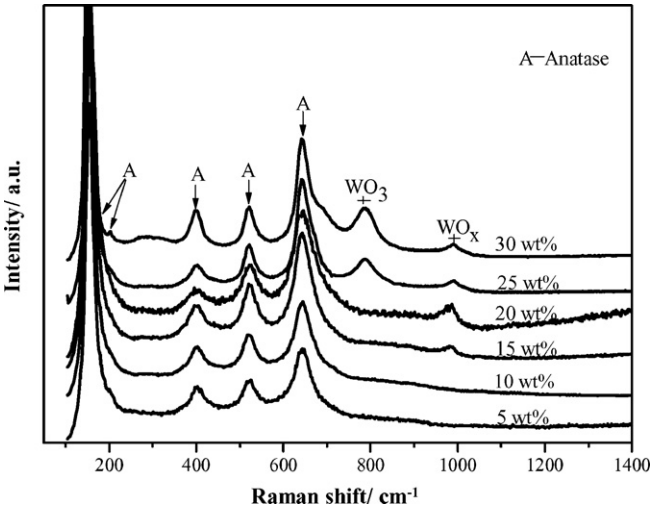

Fig. 4. Raman spectra of different WO_3/TiO_2 catalysts.

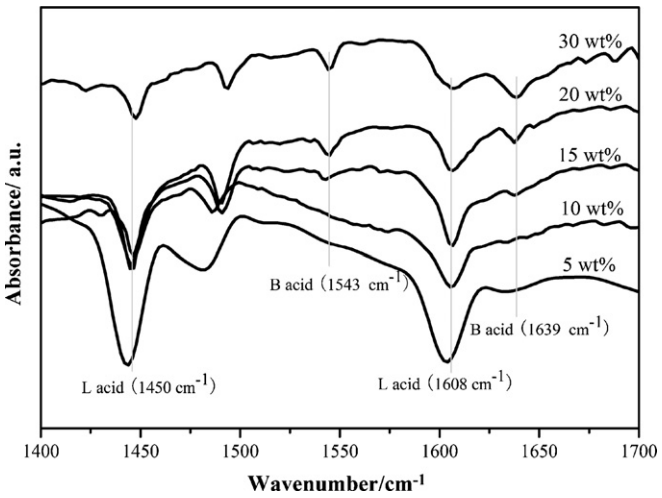

Fig. 5. IR spectra of pyridine adsorbed on different WO_3/TiO_2 catalysts.

sity increases with the increasing of WO_3 loadings up to 20 wt%, which is assigned to the W=O stretching frequencies of the tetrahedral coordinated tungsten oxide [25–27]. When the WO_3 loading approaches 25 wt%, three bands appear in the Raman spectrum at 764, 665, and 175 cm^{-1}, which are assigned to the W—O symmetric stretching mode, W—O bending mode and W—O—W deformation mode of the distorted octahedral tungsten oxide respectively [28], showing the presence of crystalline WO_3 phase [29,30]. These results are in good agreement with those of XRD patterns as shown in Fig. 2. Sohn and Park also found the formation of crystalline WO_3 for 13 wt% WO_3/ZrO_2 sample [22]. Whereas in this work, crystalline WO_3 phase was not observed for the WO_3/TiO_2 sample with the WO_3 species loading below 25 wt% at the calcination temperature of 773 K. The dispersion of WO_3 on the support is obviously dependent on the specific support, and TiO_2 microsphere is a better candidate to obtain the high dispersion of surface WO_3. That is to say that below monolayer coverage, only the surface tungsten oxide species exists on the TiO_2 microsphere surface due to the strong interaction between WO_3 and TiO_2. It seems that monolayer coverage for 25 wt% WO_3/TiO_2 has been exceeded and crystalline WO_3 is also present on the TiO_2 microsphere surface.

The Py-IR patterns of WO_3/TiO_2 catalysts with various WO_3 loadings are shown in Fig. 5. The catalysts with 5 and 10 wt% loadings exhibit IR bands at 1450 and 1609 cm^{-1}, while the samples with WO_3 loadings of 15, 20 and 30 wt% show IR bands at 1450, 1543, 1609, and 1639 cm^{-1}. The bands at 1450 and 1609 cm^{-1} are assigned to Lewis acid (L acid), and the ones at 1543 and 1639 cm^{-1} are due to Brönsted acid (B acid) [31]. With the increase of WO_3 loading, the intensity of L acid bands decreases and the one of B acid bands increases, indicating that the L acid at the surface is gradually weaken while the B acid is inchmeal enhanced.

3.2. Catalytic tests in the selective oxidation of CPE to GA

As we all known, the oxidation reaction of CPE with H_2O_2 was relatively complex. During the reaction, lots of by-products such as xide (CPO), 2-cyclopenten-1-one, 1,2-cyclopentandiol and its mono ether may be produced besides the main product of GA [12]. In this paper, only the CPE conversion and the GA yield are focused on. Table 2 summarizes the CPE conversions and GA yields over the WO_3/TiO_2 samples with different WO_3 loadings. The results show that the yield of GA increases rapidly with the increase of WO_3 loadings, when the WO_3 loading is less than 15 wt%. The GA yield increases slowly for the samples with WO_3 loading among 15 and 20 wt%, and reaches the maximum when WO_3 loading approaches

Table 2
Activity of various WO_3/TiO_2 catalysts on the selective oxidation of CPE to GA.

WO_3 loading (wt%)	H_2O_2 efficiency (%)	CPE conversion (%)	GA yield (%)
5 wt% WO_3/TiO_2	71.4	89	39
10 wt% WO_3/TiO_2	76.2	95	54
15 wt% WO_3/TiO_2	81.1	100	61
20 wt% WO_3/TiO_2	86.6	100	67
30 wt% WO_3/TiO_2	80.8	73	51

Reaction conditions: 2 ml cyclopentene, 3 ml 50% H_2O_2, 20 ml t-BuOH, 1 g WO_3/TiO_2 catalyst, T = 308 K, and t = 48 h. CPE, cyclopentene; GA, glutaraldehyde. Calcination temperature: 773 K.

20 wt%. But for the samples exceeding 20 wt%, the yield of GA decreases with further increasing of WO_3 loading. It is reasonable to think that the decrease of the activity is partly due to the conglomeration and reduce of active sites at high WO_3 loading. In addition, the phase of tungsten oxide species on the surface of TiO_2 should be considered since they possess different acid sites, which play a crucial role in their overall catalytic performance [32]. At low WO_3 loadings (normally below 15 wt%), amorphous tungsten oxide predominated and only Lewis acid character was found to be present, resulting in the yield of GA increased rapidly with increasing of WO_3 loadings [32]. At the WO_3 loading of 15–20 wt%, the tetrahedral surface tungsten oxide species (surface polytungstate species) become predominant and the interaction of WO_3 with the support becomes pretty stronger (as shown in Figs. 3 and 4). The increase of WO_3 surface coverage and the strong support interaction enhance the charge configuration to the TiO_2 microsphere support, resulting in more Brönsted acid on the surface. Therefore, both Brönsted acid sites and Lewis acid sites are present; meanwhile, the highest catalytic activity and GA yield are obtained. At high WO_3 loadings (>20 wt%), crystalline WO_3 nanoparticles (as shown in Figs. 2 and 4) formed on the TiO_2 microsphere support, Brönsted acid becomes predominant and the catalytic performance decreases correspondingly. It is primarily concluded that the surface acidity and species of catalysts play an important role in this reaction system, which needs further investigation.

4. Conclusions

To sum up, TiO_2 micospheres were fabricated by a hydrothermal precipitation procedure with $TiCl_4$ as starting material in the presence of H_2O and urea. Then a series of thermally stable WO_3/TiO_2 microsphere catalysts were successfully prepared by an ultrasonic impregnation method. The catalytic performance results show that tetrahedral surface WO_3 species with high dispersion dominate on the surface of TiO_2 support, which enhanced the Brönsted acid sites of the supported catalyst and governed the superior catalytic behavior of the WO_3/TiO_2 catalyst in the selective oxidation of CPE to GA. The optimal tungsten content was 20 wt% and the GA yield over this catalyst reached 67%, suggesting its potentially promising application in industry.

Acknowledgements

This work was supported financially by the National Nature Science Foundation of China (No. 20877013), the National High Technology Research and Development Program of China (863 Program) (No. 2007AA061402), the Major State Basic Research Development Program of China (973 Program) (No. 2007CB613306) and the Ph.D. Program Foundation of Ministry of Education of China (No. 20070141060).

References

[1] S.P. Gorman, E.M. Scott, A.D. Russell, J. Appl. Bacteriol. 48 (1980) 161–190.
[2] F.M. Collins, J. Appl. Bacteriol. 61 (1986) 247–251.
[3] P.V. Mcguken, W. Woodside, J. Appl. Bacteriol. 36 (1973) 419–426.
[4] S. Thomas, A.D. Rusell, J. Appl. Bacteriol. 37 (1974) 83–92.
[5] H. Furukawa, E. Nishikawa, T. Koyama, JP 6219546 (1987).
[6] R.H. Jin, X. Xin, D. Xue, J.F. Deng, Catal. Lett. (1999) 371–372.
[7] X. Xia, R.H. Jia, Y.G. He, J.F. Deng, H.X. Li, Appl. Surf. Sci. 165 (2000) 255–259.
[8] X.L. Yang, W.L. Dai, H. Chen, Y. Cao, H.X. Li, H.Y. He, K.N. Fan, J. Catal. 229 (2005) 259–263.
[9] X.L. Yang, W.L. Dai, R.H. Gao, H. Chen, H.X. Li, Y. Cao, K.N. Fan, J. Mol. Catal. A: Chem. 241 (2005) 205–214.
[10] X.L. Yang, W.L. Dai, C.W. Guo, H. Chen, Y. Cao, H.X. Li, H.Y. He, K.N. Fan, J. Catal. 234 (2005) 438–450.
[11] Z.Q. Zhu, W. Bian, Chin. J. Chem. Eng. 16 (2008) 895–900.
[12] R.H. Jin, X. Xin, W.L. Dai, J.F. Deng, H.X. Li, Catal. Lett. 62 (1999) 201–207.
[13] R.H. Jin, H.X. Li, J.F. Deng, J. Catal. 203 (2001) 75–81.
[14] H. Chen, W.L. Dai, J.F. Deng, K.N. Fan, Catal. Lett. 81 (2002) 31–36.
[15] W.L. Dai, H. Chen, Y. Cao, H.X. Li, S.H. Xie, K.N. Fan, Chem. Commun. 7 (2003) 892–893.
[16] L. Salvati, L.E. Makovsky, J.M. Stencel, F.R. Brown, D.M. Hercules, J. Phys. Chem. 85 (1981) 3700–3707.
[17] Y.D. Wang, Q.L. Chen, W.M. Yang, Z.K. Xie, W. Xu, D.Y. Huang, Appl. Catal. A: Gen. 250 (2003) 25–37.
[18] G. Lu, X.Y. Li, Z.P. Qu, Y.X. Wang, G.H. Chen, Appl. Surf. Sci. 255 (2008) 3117–3120.
[19] M.A. Cortés-Jácome, J.A. Toledo, C. Angeles-Chavez, J. Phys. Chem. B 109 (2005) 22730–22739.
[20] K.K. Akurati, A. Vital, J.P. Dellemann, K. Michalow, T. Graule, D. Ferri, A. Baiker, Appl. Catal. B: Environ. 79 (2008) 53–62.
[21] X.Y. Li, X. Quan, C. Kutal, Scripta Mater. 50 (2004) 499–505.
[22] J.R. Sohn, M.Y. Park, Langmuir 14 (1998) 6140–6145.
[23] M.A. Cortes-Jácome, M. Morales, C. Angeles Chavez, L.F. Ramírez-Verduzco, E. López-Salinas, J.A. Toledo-Antonio, Chem. Mater. 19 (2007) 6605–6614.
[24] S.S. Chan, I.E. Wachs, L.L. Murrell, J. Phys. Chem. 88 (1984) 5831–5835.
[25] D.G. Barton, M. Shtein, R.D. Wilson, S.L. Soled, E. Iglesia, J. Phys. Chem. B 103 (1999) 630–640.
[26] M.A. Vuurman, I.E. Wachs, A.M. Hirt, J. Phys. Chem. B 95 (1991) 9928–9937.
[27] A.K.L. Sajjad, S. Shamaila, B. Tian, F. Chen, J.L. Zhang, Appl. Catal. B: Environ. 91 (2009) 397–405.
[28] A. Anderson, Spectrosc. Lett. 9 (1976) 809–819.
[29] N.C. Ramani, D.L. Sullivan, J.G. Ekerdt, J.M. Jehng, I.E. Wachs, J. Catal. 176 (1998) 143–154.
[30] S.S. Chan, I.E. Wachs, L.L. Murrel, J. Catal. 90 (1984) 150–155.
[31] R.Q. Long, M.T. Chang, R.T. Yang, Appl. Catal. B: Environ. 33 (2001) 97–107.
[32] I.E. Wachs, T. Kin, E.I. Ross, Catal. Today 116 (2006) 162–168.